Available online at www.sciencedirect.com

ScienceDirect

Procedia CIRP 62 (2017) 15 – 20

www.elsevier.com/locate/procedia

10th CIRP Conference on Intelligent Computation in Manufacturing Engineering - CIRP ICME '16

Experimental investigation of clamping systems and the resulting change of cutting conditions while drilling carbon fiber reinforced plastics

Stefan Klotz[a],* Andreas Lepold[a], Frederik Zanger[a], Volker Schulze[a]

[a]*KIT Karlsruhe Institute of Technology, Kaiserstraße 12, 76131 Karlsruhe, Germany*

* Corresponding author. Tel.: +49-721-608-42448; fax: +49-721-608-45004. *E-mail address:* stefan.klotz@kit.edu

Abstract

Drilling is one of the most frequently applied processes for machining carbon fiber reinforced plastics (CFRP). The clamping distance influences the bending of a plane specimen when using a 4-point clamping system. In this paper, an empirical model for CFRP based on the plate theory is presented which describes the bending behavior of the specimen during the drilling process. Additionally, the influence the bending behavior exerts on the cutting thickness during drilling CFRP is described. The results show that the cutting thickness varies while drilling the material depending on the acting axial force and the current bending of the specimen.

Peer-review under responsibility of the scientific committee of the 10th CIRP Conference on Intelligent Computation in Manufacturing Engineering

Keywords: Fiber reinforced plastic; Drilling; Bending; Clamping system

1. Introduction

Fiber reinforced plastics (FRP) are suitable for multifarious applications, e.g. in the aerospace and automotive industry as well as in the leisure segment. The main reason for this lies in the high specific stiffness and strength. In addition, fiber reinforced plastics (FRP) provide design freedom for the component. Compared to the same metallic structure, the specific energy absorption capacity of carbon fiber reinforced plastics (CFRP) is between four and five times higher [1]. FRPs are usually produced in a near-net-shape process. Nevertheless, machining processes are necessary and in this case, milling and drilling are the most common ones [2].

Post-processing such as drilling leads to a weakening of the composite [3]. Moreover, the phenomenon of delamination at the upper side “peel-up” and at the underside “push-out” of the component caused by drilling is quite frequent [4]. Reducing the axial force at the entrance side and at the exit side presents one option for avoiding delamination in FRP composites [4,5]. With the combined process of circular and spiral milling and wobble milling, Schulze et al. showed that directing process forces toward the center of the workpiece decreases delamination [6]. The influence of the axial force caused by different drill geometries on delamination was investigated [7,8,9,10] as well as preventing delamination with predrilled pilot holes [11]. Drilling with a dynamically adapted feed rate was developed by Klotz et al. and shows a reduction of workpiece damage and allows a longer tool life [12].

Only little research has been executed on examining of clamping systems during machining of FRP. Uhlmann et al. investigated the influence while drilling metallic tubes with different cantilever distances. They found out that the acceleration of the beams as well as the edge layer hardness increase with rising cantilever distance [13]. The company Schmalz developed a clamping system for the variable clamping of complex workpiece geometries [14]. An optimization method for finding clamping points which held the static resilience and oscillation amplitude within some predefined boundaries was developed by Eisseler et al. [15]. A reduction of the maximum axial force during drilling cantilever beams can be observed as well as a reduction of the real feed force during the entrance of the drill tool. This leads to an increase of the total processing time. At the exit of the drill tool, the feed force temporarily increases. The use of ultrasonic assisted drilling results in a reduced deflection and

Peer-review under responsibility of the scientific committee of the 10th CIRP Conference on Intelligent Computation in Manufacturing Engineering
doi:10.1016/j.procir.2016.06.089

in a decrease of forces by 30-40%. Conversely, the surface damage increases [16,17]. Heberger et al. investigated different supports at the top layer and the bottom layer. The best results could be observed when a support plate with a predrilled hole of the same diameter as the final hole was used [18]. When a backup plate and saw or core drills are applied, higher critical feed forces can be achieved until delamination occurs [19]. The same results can be observed when using a twist drill [20]. An active backup force can reduce the surface damage at the bottom layer by about 60-80%, compared to unsupported drilling [21]. For drilling holes in FRP tubes, magnetic colloids with an applied magnetic field are pressed against the inner wall of the tube. That also leads to a reduction of damage of around 60-80% [22]. When drilling FRP metal stacks, the metallic part can be regarded as a backup plate. Qi et al. investigated the critical feed force for delamination depending on the thickness of the metal plate [23]. Capello examined the influence of supported drilling and developed a damping system which avoids a drastic increase of the feed force when the drill exits the workpiece [24]. A device which presses a plate against the upper layer leads to the reduction of peel-up delamination [25]. Luo et al. developed a model for predicting the feed force depending on the influence of workpiece stiffness and the feed rate. They divide the drilling process into three phases: The entrance phase, the full engagement phase and the exit phase of the drill. During these three phases, the feed rate changes dynamically taking into account the actual deflection of the workpiece. As a result, the uncut thickness of the material increases at the entrance and in the full engagement phase when drilling specimens with low stiffness [26]. However, the authors did not calculate the actual feed rate which occurs at the different phases of the drilling process. Klotz et al. investigated different clamping systems regarding the damage at the top and the bottom layer and showed that the tool breaks through the component and causes push-out delamination [27]. The same investigation was performed for edge milling of planar specimens with variable clamping distances [28].

Within this work, the clamping of planar specimens with a 4-point clamping system is examined. Its purpose constitutes in generating knowledge on the behavior of CFRP under uniquely defined clamping conditions and the force induced by the drilling tool. The deflection of the specimen is predicted with a specifically developed model and the local change of feed per tooth is calculated and analyzed.

2. Experiments

2.1. Experimental setup

For the drilling experiments, a 4-point clamping system is used which is comparable to the system which was shown in [27]. As can be seen in Figure 1, the specimen is clamped with four ball pressure screws on the upper side and four aluminum pins on the underside of the specimen. The clamping points are located at a distance of 10 mm to the specimen edges. The length of l_x and l_y are variable whereby different clamping distances can be configured. All drillings are located in the middle of the specimen. The distance between the drilling and clamping points was stated by l_{max}. All ball pressure screws are fixed with a tightening torque of 0.5 Nm.

In the drilling experiments, the same procedure as shown in the previous work [27,28] is used. Between each drill at the 4-point clamping system, a drill with ideal clamping condition is conducted. For these reference drills, the specimen is supported by two plates on the upper side and underside with a hole of 15 mm in diameter [27].

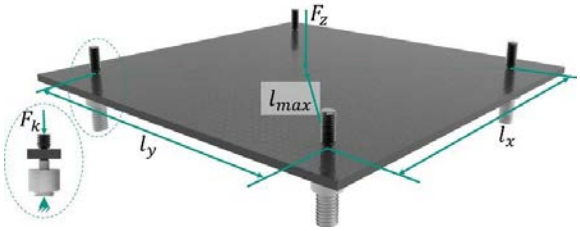

Fig. 1. Schematic drawing of the 4-point clamping system

The experiments are conducted on a Heller MC16 machining center. The multi-component dynamometer (Kistler Type 9255C) and three signal conditioner (Kistler Type 5015) are used for measuring the three orthogonal forces F_x, F_y, F_z which affect the specimen. The axial force $F_{z,Dyn}$ and torque M_z are measured with a rotating multi-component Kistler dynamometer Type 9125A at the drill. For measuring the bending moment, a potentiometric position sensor Novotechnik TR25 is used.

2.2. Material data, drill tool and process parameters

The specimens used for the experiments have the same attributes as the material used in [27]. The thickness of the plates is $h=2.5mm$. The fiber is named T620SC 24K 50C produced by Toray company. CFRP plates are pressed by the injection resin transfer molding process and consist of eight plies of endless quasi-isotropic compositions [0°/90° and +45°/-45°]. Fiber content lies at 60% and the elastic modulus at 46,100 MPa. The drilling tool for these experiments has a diameter of 10 mm and a geometry according to DIN 6539. The number of teeth is 2, the helix angle 30° and the point angle 118°. The feed rate was fixed to $v_f=300\ mm/min$ and the drill speed was fixed to $n=3{,}000\ min^{-1}$ [27].

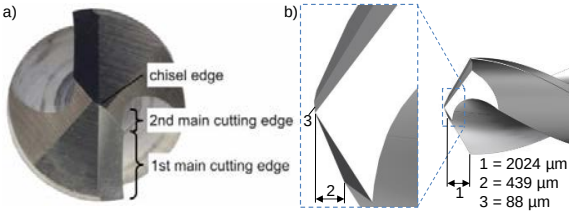

Fig. 2 a) Geometry of the drill tip; b) Height of the cutting edge at the drill tip

As Figure 2 (a) demonstrates, the main cutting edge can be divided into two sections, the first main cutting edge and the

second main cutting edge. Figure 2 (b) also illustrates the length of the first main cutting edge (1), the length of the second main cutting edge (2) and the length of the chisel edge (3).

3. Modeling of workpiece deflection and cutting conditions

The stiffness of the material can be described by *N*, depending on the elastic modulus ε and the Poisson's ratio ν, cf. formula (1) [29].

$$N = \frac{\varepsilon * h^3}{12 * (1-\nu^2)} \quad (1)$$

The theoretical deflection w_t of a point load on a rectangular plate was described by Marcus (Eq. 2). For a central point load, he set a fixed value α=*0.155129* and *P* showed the axial force for the entire drilling process in dependence of the time [30].

$$w_t = \alpha * \frac{P * l_x^2}{N} \quad l_x \geq l_y \quad (2)$$

Stiglat & Wippel [31] also used Eq. (2) but, depending on different clamping conditions, they calculated different values for α. It follows that α is a process variable which denotes the boundary conditions for the clamping and the aspect ratio of the rectangular plate l_x/l_y. Therefore, in this publication the method of Stiglat & Wippel [31] is used and α empirically adapted to the used CFRP material. An adequate result can be obtained when comparing the measured deflection *w* and the calculated deflection w_t.

Luo et al. [26] showed, that the derivation of deflection is equal to the speed of deflection. Consequently, Eq. (3) describes the speed of the deflection:

$$w' = \frac{dw}{dt} \quad (3)$$

Based on machining parameters, the predefined feed rate per cutting tooth $f_{z,p}$ is described by Eq. (4):

$$f_{z,p} = \frac{v_f}{n * z} \quad (4)$$

Here, v_f is the adjusted feed speed, *n* represents the drill speed and *z* the number of teeth. Caused by the deflection of the specimen, the real feed rate per cutting edge varied during the drilling process [26]. The real dynamic feed per tooth is defined as:

$$f_{z,Dyn} = \frac{v_f - w'}{n * z} \quad (5)$$

Due to the deflection of the specimen, there is a difference between the theoretical cutting depth b_t (Eq. 6) and the experimental cutting depth b_e (Eq. 7) over time [26].

$$b_t = h - v_f * t \quad (6)$$

$$b_e = h - (v_f * t - w_t) \quad (7)$$

Caused by arising problems when differentiating the modelled and the real deflection of the specimen, an FFT analysis is performed for the measurement results of the potentiometric position sensor and the axial force $F_{z,Dyn}$. As a result of the FFT analysis, it can be shown that frequencies higher than 25 Hz lead to problems when using the analyzing method. In consequence of the FFT analysis, a Savitzky-Golay filter with 5,000 neighboring date points and a polynomial of the second order is used. This results in smoothed data for the real deflection *w* and the modelled deflection w_t.

4. Results

4.1. Theoretical bending

Based on the findings of Stiglat & Wippel, an empirical model has been adapted which describes the profile of the deflection for CFRP over the entire drilling process [31]. Therefore, experiments to determine α are conducted at the beginning. With the method of least squares, different values for different clamping conditions are assigned to the variable α. The values depending on the various clamping conditions are shown in Table 1.

Table 1. Empirical results for α and the mean squared error for different clamping conditions

l_x/l_y	*1/4*	*1/2*	*3/4*	*1*
Empirical results for α	0.03829	0.02069	0.01973	0.0231
Mean Squared Error (10^{-3})	14.8	1.98	0.0449	0.1986

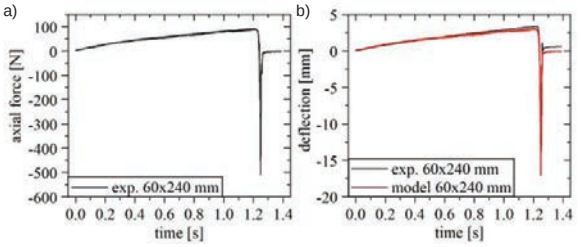

Fig. 3. Axial force of the drilling experiment 60x240 mm (a), Quality of the theoretical bending for clamping condition l_x/l_y = 1/4 (b)

Figure 3 shows the axial force (a) and the quality of the theoretical deflection w_t in comparison to the measured deflection *w* of the reference group (b) with clamping conditions (l_x/l_y): ¼. In Fig. 3 (a), a catastrophic breakthrough of the drill at 1.25 s can be seen. The axial force at this point is about -511 N. The empirical model of the deflection w_t describes the profile of the deflection of the workpiece over the entire drilling process with a good approximation (Fig. 3 b). In Fig. 3 (b), the slope of w_t at the beginning is nearly the same as *w*. Shortly before the drill tool breaks through the specimen, the deviation is less than 8% and the mean squared error (MSE) is 0.0148. The MSE for the other clamping

conditions is depicted in Table 1. It shows that the model is in good agreement with the experimental deflection of the specimen in terms of the aspect ratios.

4.2. Drilling steps

Fig. 4. illustrates that the entire drilling process for the used drill tool can be subdivided into seven steps (1-7). First of all, the chisel edge penetrates the specimen (1) and deflection starts. In the present case, after the drill reaches a depth of 0.0878 mm, the second main cutting edge starts cutting the material (2). When the second main cutting edge is completely engaged, the first main cutting edge begins machining (3). At step (4) the first main cutting edge is completely engaged. The drill is in full contact until the chisel edge leaves the workpiece (5). In the next two steps, the second main cutting edge exits the workpiece (6) and the first cutting edge enters the workpiece (7). When the first main cutting edge leaves the specimen completely, the entire drilling process is completed.

Caused by the total length of the drill tip (2.551 mm) and the thickness of the specimen (*h=2.5 mm*), the chisel edge gets through the workpiece before the first main cutting edge is completely engaged. Therefore Step 4 does not exist in our case.

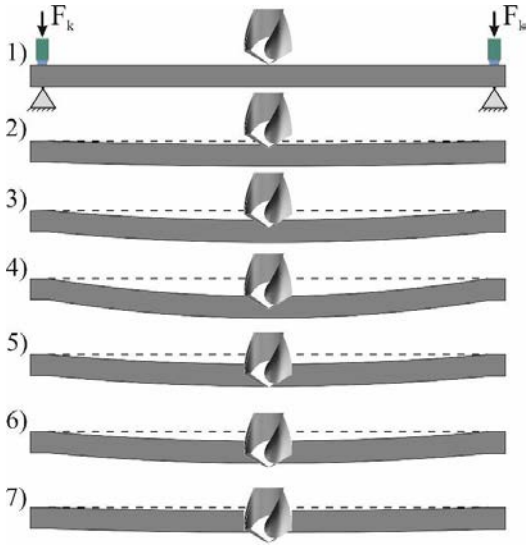

Fig. 4. Drilling steps for the entire drilling process

In Fig. 5, the axial force (a) and the drilling depth (b) under clamping conditions 60x60 mm are shown. In Fig. 5 (b), the drilling depth when drilling a hole with an ideal clamping condition (infinite stiffness) is compared to the experimental drilling depth considering the workpiece deflection. The explained steps from Fig. 4 are marked in Fig. 5. The material thickness *h=2.5 mm* and the point where the drilling tool has completely drilled through the specimen (line approx. 5.05 mm) are also shown. This length can be calculated by summing up the material thickness and the height of the drill tip. The deviation of the curve progression between the real clamping conditions 60x60 mm and the ideal clamping conditions is quite small. Only after the chisel edge has completely entered the specimen and the second main cutting edge starts machining, the workpiece gets deflected (Fig. 5 step 1 and 2). After about 0.516 s the chisel edge exits the workpiece and after 0.538 s it is completely resigned from the workpiece (Figure 5, step 5). Compared to ideal clamping conditions, a deflection of 0.08 mm prevails at this point and the axial force is about $F_{z,Dyn}=87$ *N*. The entire drilling process is completed after a total of 1.01 s, the same period of time as under ideal clamping conditions.

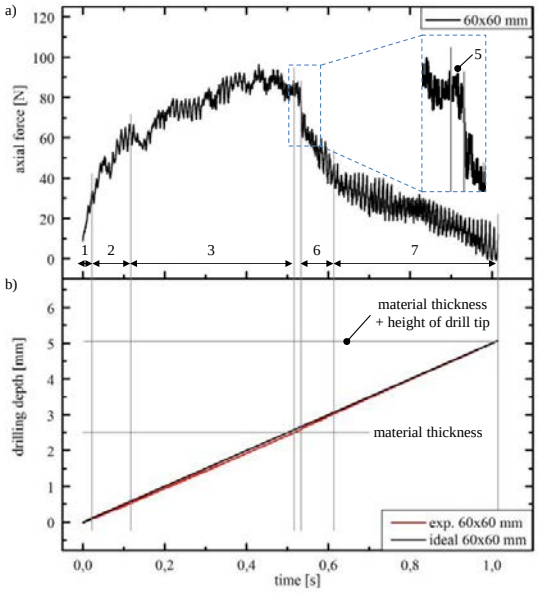

Fig. 5. Axial force for clamping conditions 60x60 mm (a); drilling depth for ideal and experimental clamping conditions 60x60 mm (b)

In Fig. 6, the axial force (a) and the drilling depth (b) under clamping conditions 120x120 mm are shown similar to the clamping distance of 60x60 mm in Fig. 5. As can be seen in Figure 6 (a), the tool has a catastrophic breakthrough. This phenomenon was shown by [27] at a clamping length which is equal or higher than 80x80 mm. It can be seen that the tool breaks through the specimen when the first main cutting edge starts to exit the specimen (step 7). When comparing Figure 6 (a) and (b) it can be seen that, at the point where the tool breaks through the workpiece, the uncut thickness of the material at the wall of the drill is about 2.02 mm.

Under ideal clamping conditions, the chisel edge exits the workpiece in 0.5 s. As seen in Figure 6 (b), the intersection of mark (5) and the thickness *h=2.5 mm* is about 0.58 s. At this time, the chisel edge leaves the specimen. Compared to ideal clamping conditions, a deflection of 0.40 mm prevails at this point and the axial force $F_{z,Dyn}$ has reached its maximum peak of about 87 N, the same value as shown in Fig. 5. This time delay, until the chisel edge exits the specimen, is caused by a deflection of the specimen. With the beginning of step (7), the slope of the real drilling depth increases drastically. When the first main cutting edge exits the specimen, the workpiece gets lifted up caused by the grooves of the drill. Step (7) is completed after a period of 0.011 s. At this time, the axial

force has reached its minimum peak at about -570 N. With the help of the relative motion caused by the active pull-up by the grooves of the drilling tool, the feed reached $v_{f,exp} \approx 11{,}100\ mm/min$ at this short time period (adjusted $v_f = 300\ mm/min$). When the grooves clasp into the specimen and pull it up, the drilling process is completed after a half turn of the drill.

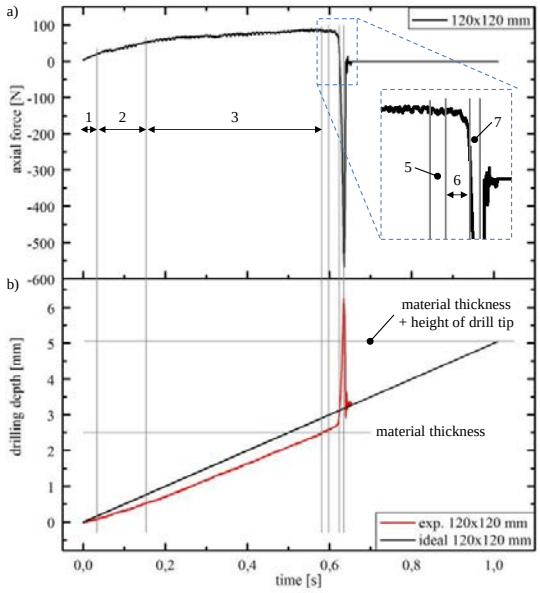

Fig. 6. Axial force for clamping conditions 120x120 mm (a); drilling depth for ideal and experimental clamping conditions 120x120 mm (b)

4.3. Dynamic feed rate per cutting edge

The speed of deflection can be calculated when using Eq. (3) and the resulting feed per tooth can be calculated when using Eq. (5). These approaches are valid until the first main cutting edge is in full contact with the specimen (Fig. 4 (4)). Fig. 7 (a) shows the deflection for three clamping conditions and compares the results with the modeled deflection. When differentiating the modeled deflection by using Eq. (3), the speed of deflection can be calculated (Fig. 7 (b)). It is evident that the slope of the speed of deflection initially increases. For all clamping distances, the highest speed of deflection is reached when the chisel edge and the second main cutting edge join the specimen. For clamping conditions 120x120 mm, the maximum peak is around 115 mm/min and reduces the preset feed rate by about 30%. After that, the speed of deflection remains constant at a lower level and falls back to zero when the first main cutting edge is in full contact with the workpiece. When using Eq. (5), the real feed per tooth can be calculated (Fig. 7 (c)). It can be seen, that the predefined feed per tooth $f_{z,p} = 0.05\ mm$ was reached only at the beginning of the breakthrough of the drill at higher clamping distances, with the exception of small clamping distances such as 40x40 mm. In this experiment, the feed per tooth corresponds to the predefined feed per tooth after the chisel edge and the second main cutting edge are in contact with the specimen. However, at higher distances l_x/l_y the feed per tooth remains constantly below 0.05 mm and reaches $f_{z,p}$ only with beginning of the breakthrough of the chisel edge. This is due to the lower stiffness of the specimen of these clamping conditions. It is obvious that the predefined feed per tooth can only be reached when the feed of deflection is zero.

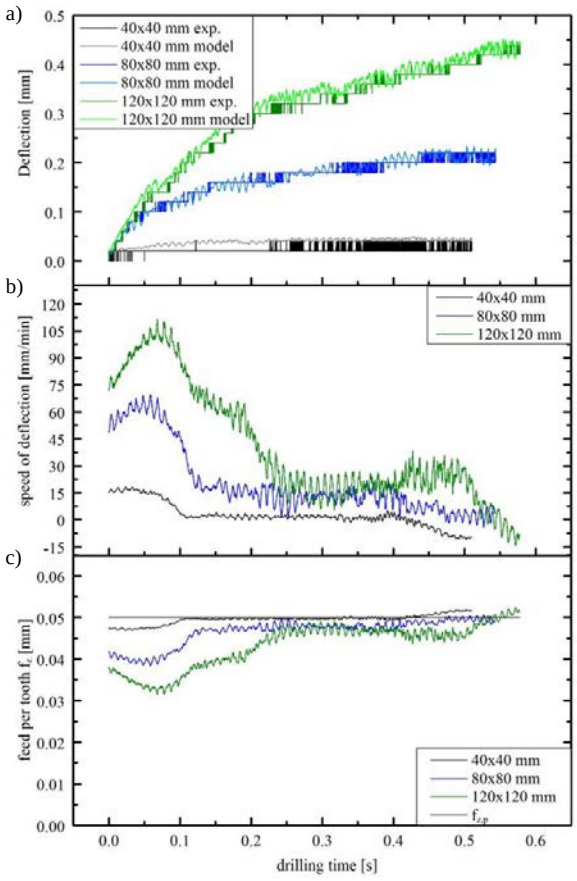

Fig. 7. Comparison data among deflection (a), speed of deflection (b) and feed per tooth (c) for different clamping conditions for the drilling process until the breakthrough

5. Conclusion and outlook

Based on the analysis of the conducted experiments the following results can be determined:

- As a result of the experiments, the relationship between the deflection and the influencing axial force could be determined. In addition, an empirical model w_t has been adapted based on the plate theory which describes the profile of the deflection of the CFRP workpiece throughout the entire drilling process with good approximation.

- It can be shown that at the beginning of the drilling process the highest speed of deflection occurs. Depending on the clamping condition, the real feed was reduced up to 30%. This shows that the cutting conditions vary during the entire drilling process.

- It has been provided that for the entire drilling process the feed per tooth is variable and differs from the predefined feed per tooth $f_{z,p}$ depending on the clamping conditions. In this context, the variable feed per tooth $f_{z,Dyn}$ was calculated.

- It has been shown that $f_{z,Dyn}$ decreases at the beginning of the drilling process. For different clamping conditions it has been provided that, when the chisel edge and the second main cutting edge are fully engaged, $f_{z,Dyn}$ is tending to $f_{z,p}$.

In further experiments the empirical model should be verified for further clamping conditions, different material thicknesses and layer setups. Furthermore, the combination of dynamic parameter adaption and the combination with different clamping systems will be examined. With this result, it can be ensured that constant parameters can be reached when drilling with flexible clamping conditions. This supports the approach presented in [12]. With this method also the tool lifetime can be increased.

Acknowledgements

This project is funded by the EU through the program “European Funds for Regional Development” as well as the state government of Baden-Wuerttemberg in Germany. Administrative agency of this program is the Ministry of Rural Development, Food and Consumer Protection. More Information: www.rwb-efre.baden-wuerttemberg.de.

References

[1] Schürmann Helmut. Konstruieren mit Faser-Kunststoff-Verbunden. 2nd ed. Berlin, Heidelberg: Springer-Verlag Berlin Heidelberg; 2007.
[2] König W, Wulf Ch, Graß P, Willerscheid H. Machining of Fibre Reinforced Plastics. In: Annals of the CIRP Vol. 34/2/1985; 1985. p. 537-548.
[3] Langella A, Durante M. Comparison of Tensile Strength of Composite Material Elements with Drilled and Molded-in Holes. In: Composite Materials 15 (4-6); 2008. p. 227–239.
[4] Ho-Cheng H, Dharan CKH. Delamination During Drilling in Composite Laminates. In: Journal of Engineering Industry (112); 1990. p. 236-239.
[5] Mohan NS, Kulkarni SM, Ramachandra A. Delamination analysis in drilling process of glass fiber reinforced plastic (GFRP) composite materials. In: Journal of Materials Processing Technology 186 (1-3); 2007. p. 265–271.
[6] Schulze V, Becke C, Weidenmann K, Dietrich S. Machining strategies for hole making in composites with minimal workpiece damage by directing the process forces inwards. In: Journal of Materials Processing Technology 211; 2011. p. 329-338.
[7] Hocheng H, Tsao CC. Effects of special drill bits on drilling-induced delamination of composite materials. In: International Journal of Machine Tools & Manufacture 46; 2006. p. 1403-1416.
[8] Durao LMP, Goncalves DJ, Tavares JMR, de Albuquerque VHC, Marques AT. Comparative analysis of drills for composite laminates. In: Journal of Composite Materials 46 (14); 2012. p 1649-1659.
[9] Heisel U, Pfeifroth T. Influence of Point Angle on Drill Hole Quality and Machining Forces When Drilling CFRP. 5th CIRP Conference on High Performance Cutting 2012. In: Procedia CIRP Vol 1; 2012. p. 471–476.
[10] An Q, Xu J, Ca X, Chen M. Experimental investigation on drilling force and hole quality when drilling of T800S/250F CFRP laminate. In: Advanced Materials Research 797; 2013. p. 155-160.
[11] Tsao CC, Hocheng H. The effect of chisel length and associated pilot hole on delamination when drilling composite materials. In: International Journal of Machine Tools & Manufacture 43; 2003. p. 1087–1092.
[12] Schulze V, Zanger F, Klotz S. Verschleißbedingte Parameteranpassung bei der Bohrungsherstellung in faserverstärkten Kunststoffen. In: Wanner A, Weidenmann K, editors. Verbundwerkstoffe: Conference proceedings, Karlsruhe; 03-05 July 2013. p. 658–664.
[13] Uhlmann E, Gebhard S, Kaulfersch F, Löser M. Labile Werkstückaufspannung beim Bohren. Einfluss der Spannsituation beim Bohren schwingungsbelasteter Bauteile. In: VDI-Z Integrierte Produktion 156 (1/2); 2014. p. 48–50.
[14] Schmalz K, Günther K. Chancen für den Unterdruck. Markt und Trends in der Vakuumtechnik. In: Fluidtechnik; 2013. p. 72–75.
[15] Eisseler R, Jakob P, Schaal M, Weiland S. Bohren von CFK. Einfluss der Werkstückeinspannung. 3. IFW-Tagung Bearbeitung von Verbundwerkstoffen - Spanende Bearbeitung von CFK. Stuttgart, editors Institut für Werkzeugmaschinen; 22.10.2013.
[16] Kaufeld M, Lissek F, Bergmann JP. Bearbeitungskriterien für die Zerspanung labiler CFK-Strukturen. Aufs Abstützen kommt es an. In: WB Werkstatt + Betrieb 2013 (12); 2013. p. 36–40.
[17] Lissek F, Kaufeld M, Bergmann JP. Spanende Bearbeitung von labilen CFK-Bauteilen. In: MM MaschinenMarkt 2015 (39); 2015. p. 80–84.
[18] Heberger L, Nissle S, Gurka M, Kirsch B, Aurich JC. Qualitätssicherung von Bohrungen in Faserkunststoffverbunden. Untersuchung des Einflusses der Einspannstrategien. In: wt Werkstattstechnik online 105 (7/8); 2015. p. 501–507.
[19] Tsao CC, Hocheng H. Effects of exit back-up on delamination in drilling composite materials using a saw drill and a core drill. In: International Journal of Machine Tools and Manufacture 45 (11); 2005. p. 1261–1270.
[20] Tsao CC. Effects of Passive Backup Force on Delamination in Drilling Composite Materials Using Twist Drill. In: AMR 479-481; 2012. p. 213–216.
[21] Tsao CC, Hocheng H, Chen YC. Delamination reduction in drilling composite materials by active backup force. In: CIRP Annals - Manufacturing Technology 61 (1); 2012. p. 91–94.
[22] Hocheng H, Tsao CC, Liu CS, Chen HA. Reducing drilling-induced delamination in composite tube by magnetic colloid back-up. In: CIRP Annals - Manufacturing Technology 63 (1); 2014. p. 85–88.
[23] Qi Z, Zhang K, Li Y, Liu S, Cheng H. Critical thrust force predicting modeling for delamination-free drilling of metal-FRP stacks. In: Composite Structures 107; 2014. p. 604–609.
[24] Capello E. Workpiece damping and its effect on delamination damage in drilling thin composite laminates. In: Journal of Materials Processing Technology 148 (2); 2004. p. 186–195.
[25] Sadat AB. Preventing Delamination when drilling Graphite/Epoxy Composite. In: Engineering Systems Design and Analysis 2; 1994. p. 9–18.
[26] Luo B, Li Y, Zhang K, Cheng H, Liu S. Effect of workpiece stiffness on thrust force and delamination in drilling thin composite laminates. In: Journal of Composite Materials; 2015. p. 1-9.
[27] Klotz S, Gerstenmeyer M, Zanger F, Schulze V. Influence of clamping systems during drilling carbon fiber reinforced plastics, 2nd CIRP Conference on Surface Integrity (CSI). In: Procedia CIRP 13; 2014. p. 208-213.
[28] Klotz S, Zanger F, Schulze V. Influence of clamping systems during milling of carbon fiber reinforced composites. New Production Technologies in Aerospace Industry - 5th Machining Innovations Conference (MIC 2014). In: Procedia CIRP 24; 2014. p. 38-43.
[29] Hake E, Meskouris K. Statik der Flächentragwerke: Einführung mit vielen durchgerechneten Beispielen. 2nd ed. Berlin: Springer; 2007.
[30] Marcus H. Die Theorie elastischer Gewebe und ihre Anwendung auf die Berechnung biegsamer Platten: Unter besonderer Berücksichtigung der trägerlosen Pilzdecken. Berlin: Springer; 1924.
[31] Stiglat K, Wippel H. Platten: Plattenstreifen, punktgestützte Platten, zwei-, drei- und vierseitig gestützte Platten, elastisch gestützte Platten, Dreieckplatten, Kreisplatten, drillweiche Platten, Platten mit unterbrochener Stützung, Platten auf elastischer Bettung. 3rd ed. Berlin: W. Ernst; 1983.